International Journal of Astrobiology

cambridge.org/ija

Solar system exposure to supernova γ radiation

G. Robert Brakenridge

INSTAAR, University of Colorado, 4001 Discovery Drive, Boulder CO 80303, USA

Research Article

Cite this article: Brakenridge GR (2021). Solar system exposure to supernova γ radiation. *International Journal of Astrobiology* **20**, 48–61. https://doi.org/10.1017/S1473550420000348

Received: 26 April 2020
Revised: 9 August 2020
Accepted: 12 October 2020
First published online: 4 November 2020

Author for correspondence:
G. Robert Brakenridge,
E-mail: Robert.Brakenridge@Colorado.edu

Abstract

Planetary habitability may be affected by exposure to γ radiation from supernovae (SNe). Records of Earth history during the late Quaternary Period (40 000 years to present) allow testing for specific SN γ radiation effects. SNe include Type Ia white dwarf explosions, Type Ib, c and II core collapses, and many γ burst objects. Surveys of galactic SNe remnants offer a nearly complete accounting for this time and including SN distances and ages. Terrestrial changes in records of the cosmogenic isotope ^{14}C are here compared to SN-predicted changes. SN γ emission occurs mainly within 3 years; average per-event total emissions of 4×10^{49} erg are used for comparison of close events There are 18 SNe ≤ 1.5 kpc, and brief ^{14}C anomalies are reported for eight of the closest. Four are notable (BP is year before 1950 CE): the older Vela SNR and an abrupt 30‰ del ^{14}C rise at 12 740 BP; S165 and a 20‰ rise at 7431 BP; Vela Jr. and a 14‰ rise at 2765 BP; and HB9 and a 9‰ rise at 5372 BP. Rapid-increase anomalies in ^{14}C production have been attributed to cosmic rays from exceptionally large solar flares. However, the proximity and ages of these SNe, the probable size and duration of their γ emissions, the predicted effects on ^{14}C, and the agreement with ^{14}C records together support SNe causation. Also, the supposed solar-caused ^{14}C anomalies at CE 774 and 993 may instead have been caused by the SNe associated with the *G190.9-2.2* and *G347.3-00.5* remnants. Both are of appropriate age and distance.

Introduction

Understanding the habitability of planets in the Milky Way includes evaluation of exposure to high-energy photon radiation from supernovae (SNe) and γ ray bursts (GRBs) (Piran and Jimenez, 2014; Gowanlock, 2016). The predicted effects of hard photon radiation on Earth include temporarily elevated levels of cosmogenic isotopes such as ^{14}C, ^{10}Be and ^{36}Cl, ionization of N species in the atmosphere, depletion of the ozone layer, increased UV radiation at the Earth's surface and delivery of fixed N to the Earth's surface. There is a rich literature describing these potential effects (Terry and Tucker, 1968; Ruderman, 1974; Clark *et al.*, 1977; Rood *et al.*, 1979; Thorsett, 1995; Scalo and Wheeler, 2002; Gehrels *et al.*, 2003; Melott *et al.*, 2003, 2005; Thomas *et al.*, 2005; Galante and Horvath, 2007; Martín *et al.*, 2009; Thomas, 2009; Horvath and Galante, 2012; Gowanlock, 2016). If sufficiently intense, the radiation events can also affect other solar system atmospheres and surfaces (Duggan *et al.*, 2001; Scalo and Wheeler, 2002; Fox *et al.*, 2017).

In this regard, records of the Earth's paleoenvironmental history during the late Quaternary Period (40 000 years BP to present) allow testing of hypotheses concerning the possible terrestrial effects (Brakenridge, 1981). On Earth, marine, lake and ice cores, speleothems, and tree ring records provide opportunities to locate and measure the traces, including through the use of cosmogenic isotopes produced in the atmosphere. At present, even the γ radiation from distant galactic magnetar flares and from GRBs in other galaxies creates measurable terrestrial ionosphere changes (Fishman and Inan, 1988; Inan *et al.*, 2007; Tanaka *et al.*, 2008) and neutron thermalization effects from lightning-produced γ are also observed (Carlson *et al.*, 2010). Using tree rings, it is possible to assay relatively small changes in the cosmogenic isotope ^{14}C on an annual or near-annual basis over thousands of years (Damon *et al.*, 1995; Miyake *et al.*, 2012; Miyake *et al.*, 2016). Thus, SN radiation events of different sizes can be detected and measured: if they can be separated from the changes produced by other environmental variables.

To understand probable exposure history from SNe, the expected emissions, distances and ages must be estimated or measured. In this regard, the sizes and energy cross-sections of γ radiation from 'typical' SNe in other galaxies, of various classes, and from GRBs are increasingly constrained, through theory, modelling and direct observations (Matz *et al.*, 1988; Churazov *et al.*, 2015; Wang *et al.*, 2019*a*, 2019*b*). Also, detailed and nearly complete inventories of in-galaxy prehistoric SNe as detected by their remnant nebulae (SNRs) and/or remnant compact objects are available (Farrand and Safi-Harb, 2012; Zhu and Tian, 2013; Green, 2019). The ages and distances of most galactic SNRs in this time period are constrained by

© The Author(s), 2020. Published by Cambridge University Press

CAMBRIDGE UNIVERSITY PRESS

observations, and in many cases, the sizes of progenitor stars and the total explosion energies have been determined.

SNRs are strong radio emitters and most objects within the Milky Way are believed to have already been detected: although newly discovered ones are occasionally reported (Foster *et al.*, 2013; Gao *et al.*, 2020). Thus, the galactic inventory may be nearly complete for the past ~40 000 years (Green, 2019). The remnant nebulae expand through time and eventually merge into the interstellar medium: 40 000 years appears to be a practical maximum age limit for comparisons of known SNe to observed terrestrial responses. There can now be assembled a list of candidate events that may have been sufficiently intense to have effected terrestrial environmental changes. Their Earth-incident γ fluences and ages provide a chronology of late Quaternary solar system exposure, and this can be compared to terrestrial records of relevant changes. For the latter objective, this paper emphasizes the cosmogenic and radiogenic isotope ^{14}C as a sensitive indicator.

Methodology

Presently, any SNe causation for significant terrestrial changes during this time period is unproven. Some workers conclude that massive solar energetic particle events (SEPs) must instead be invoked to explain observed abrupt increases in atmospheric 14C production (Usoskin *et al.*, 2013; Dee *et al.*, 2016). This even though the most intense solar flare in history, the Carrington corona mass ejection, left no ^{14}C traces (Jull *et al.*, 2020). Also, in at least two cases, possible SNe causation for measured abrupt ^{14}C changes has been dismissed because no possibly associated SNRs were thought to exist (Dee *et al.*, 2016). Plausible SN candidates are now available for both (see text below and Zhu and Tian, 2013). This emphasizes the need for a comprehensive chronology of nearby SNe events and expected emission fluences during this time period.

There may be no reason to exclude either solar or SNe causation for changes in the detailed late Quaternary records of the cosmogenic isotopes: 'It is clear that there are several types of rapid events in the $\Delta^{14}C$ record' (Jull *et al.*, 2020). In this regard, predictive capability is an important criterion for the utility of any causal hypothesis. If secure linkages are established for even a few SNe/terrestrial response events, then, given the reservoir of dozens of known SNe, this causal understanding can help guide further work and including investigation of other predicted effects. This paper provides evidence for a hypothesis that offers some explanatory power and also utility for prediction. Thus, if: (1) an SN is known to have occurred, within uncertainty, at a particular time; (2) its emitted energy was likely of sufficient size and spectral characteristics to have caused a predicted terrestrial response, and (3) there is documentation in terrestrial records at that time of such a response, then the hypothesis of SN causation is viable and must be retained to guide further work.

This paper: (1) inventories all nearby SNRs that are <40 000 years in age, (2) compiles the relevant observational statistics including distances and ages, (3) constrains the probable emission energies from recent SN theory, modelling and observational results, and (4) compares the resulting solar system radiation history to relevant terrestrial records that could record the predicted changes.

Locating nearby supernovae

Three comprehensive radio and high-energy catalogues of SNRs (Safi-Harb *et al.*, 2012; Pavlovic *et al.*, 2014; Green, 2019) were interrogated to identify objects $<5 \times 10^4$ years in age and <1.5 kpc in distance, providing 18 objects (Table 1). Although some ages for radio SNRs are based on radio surface brightness/remnant diameter (Σ–D) and D-age relations, these are calibrated using measured radial expansion velocities and other methods. Their precision is known to be low (±25%) (Pavlovic *et al.*, 2014). Thus, these were used only when other more-direct estimates were not available. Where uncertainty values are published, they are included in Table 1; otherwise an uncertainty of ±25% (standard error) is assumed. All uncertainties are carried through to incident fluence (energy/unit area) and also ^{14}C production calculations (see following sections).

There are also approximately 20 poorly-constrained SNR compact objects in the high-energy compilation (Safi-Harb *et al.*, 2012) for which no distances or ages are available. These were excluded for the purpose of this paper and because it is unlikely that any of these are close, relatively young and of importance to the present analysis. For convenient reference, the common names of the SNRs are also provided in Table 2.

Table 1, as described further below, adopts 4×10^{49} erg as a reasonable 'typical' total γ (mainly 70 MeV to 10 GeV): over 3 years, including prompt relativistic shock breakouts, any intercepted jetted emission and sustained emission. This is for comparison of SNe events of varying distances. However, intrinsic intensities, duration and γ cross-sections of Milky Way SNe may vary significantly. In this regard, the distances of the SNE of most interest vary from 0.25 to 1 kpc, which using the inverse square law provides a 16× luminosity factor if γ from each event was identical. The intrinsic energy uncertainties may be reduced in the future by more observation and analysis of the individual candidate SNR characteristics, such as calculated total explosion energies and progenitor star masses; a more detailed consideration is provided below.

The distances in Table 1 are based on a variety of observational methods: proper motions, shock and radial velocities, H_I absorption and polarization, kinematic spectral line observations and association with star fields measured via parallax. Accuracies vary; for kinematic distances, the uncertainties may be <30%; for distances from X-ray fitting, they may be >50% (Zhu and Tian, 2013). Where uncertainties are not available for particular objects, a ±25% value is assumed and represents an approximate average of the published uncertainties (Table 1).

Available age estimates are partially dependent on measured or estimated distances. Those in Table 1 include ages from empirical SNR radio surface brightness/remnant diameter Σ–D and D–age relations, and also from measured radial expansion velocities; the latter may be more accurate. Where uncertainty values are published, they are included in Table 1. The most recent observational findings for the SNe are used in each case.

Constraints over typical SNe γ emission energies

Varying intrinsic emission energies may strongly affect the accuracy of the predicted terrestrial SN γ fluences provided in Table 1. Related research using the new satellite observatories as applied to extragalactic SNE is rapidly expanding and is critical to understanding terrestrial and solar system exposure.

SNe are diverse and created by different types of explosions (e.g. those associated with Type 1A white dwarf binaries and Type II massive or supermassive progenitor stars). Such diversity also occurs for their observed γ emissions and associated spectral cross-sections: although these can be remarkably uniform within

https://doi.org/10.1017/S1473550420000348 Published online by Cambridge University Press

https://doi.org/10.1017/S1473550420000348 Published online by Cambridge University Press

Table 1. Distances, Earth-incident γ (using 4×10^{49} erg total γ SN emission), ages, predicted ^{14}C production and measured ^{14}C rise (reported as $+\Delta^{14}C$) within the time intervals for 18 of the closest SNe

Catalogue number	Distance (kpc)	Total γ (erg cm^{-2})	SN age (BP) (a cm^{-2} s^{-1})	Predicted ^{14}C production	Measured $\Delta^{14}C$ anomaly and age range
G263.9-03.3	0.25 ± 0.03	$1.1–1.7 \times 10^6$	14 500 ± 1500	4.4–7.1	+40‰, 12 745–12 630 BP
G330.0+15.0	0.32 ± 0.17	$0.3–3.7 \times 10^6$	23 000 ± 8000	1.4–15.3	+21‰, 22 500–22 360 BP
G114.3+00.3	0.70 ± 0.35	$0.8–6.8 \times 10^5$	~7700	0.3–2.8	+20‰, 7431–7421 BP
G266.2-1.2	0.70 ± 0.25	$0.9–4.1 \times 10^5$	3800 ± 1400	0.4–1.7	+13‰, 2765–2749 BP
G074.0-08.5	0.74 ± 0.03	$0.6–5.2 \times 10^5$	15 000 ± 5000	0.6–0.7	14 722–14 712 BP
G160.9+02.6	0.80 ± 0.40	$0.8–2.3 \times 10^5$	5500 ± 1500	0.2–2.2	+9‰, 5372–5362 BP
G106.3+02.7	~0.80	$0.5–1.5 \times 10^5$	~10 000	0.3–1.0	+12‰, 10 255–10 220 BP
G040.5+00.5	~1.00	$0.5–1.5 \times 10^5$	~20 000	0.2–0.6	
G190.9-2.2	~1.00	$0.5–1.5 \times 10^5$	~1550	0.2–0.6	+15‰, 1176–1166 BP
G152.4-2.1	~1.00	$0.5–1.5 \times 10^5$	~6900	0.2–0.6	
G107.5-1.5	~1.10	$0.4–1.1 \times 10^5$	4500 ± 1500	0.2–0.6	+20‰, 4880–4820 BP
G127.1+0.5	~1.15	$0.3–1.3 \times 10^5$	~25 000	0.2–0.5	+46‰, 26 200–25 520
G205.5+0.5	1.20 ± 0.40	$0.3–1.0 \times 10^5$	90 000 ± 60 000	0.1–0.5	
G347.3-00.5	1.30 ± 0.40	$1.2–4.1 \times 10^5$	1840 ± 260	0.1–0.4	+9‰, 957–947 BP
G180.0-1.7	$1.30^{+0.22}_{-0.16}$	$3.8–6.8 \times 10^4$	30 000 ± 4000	0.2–0.3	
G260.4-3.4	1.30 ± 0.30	$3.3–8.4 \times 10^4$	1990 ± 150	0.1–0.3	
G119.5+10.2	1.40 ± 0.30	$2.9–6.9 \times 10^4$	~13 000	0.1–0.3	
G327.6+14.5	~1.56	$2.2–6.1 \times 10^4$	944 (SN 1006)	0.1–0.3	+5–9‰, 942–933 BP

^{14}C production is based on 130 atoms per SN-generated γ erg. The γ fluence is divided by 4 to adjust the distance-corrected total SN γ/cm^2 to a spherical Earth. The energies and production ranges are based on the distance uncertainties. The $\Delta^{14}C$ results use the higher temporal resolution data when available, as described in the text. Ages are years before present (BP, before CE 1950). All errors are expressed as standard errors; a ±25% error is assumed if not otherwise provided.

Table 2. SNR catalogue numbers and names

G263.9-03.3	Vela X Y Z
G330.0+15.0	Lupus Loop
G114.3+00.3	S165
G266.2-1.2	Vela Jr.
G074.0-08.5	Cygnus Loop
G160.9+02.6	HB9
G106.3+02.7	Boomerang
G040.5+00.5	G040.5+00.5
G190.9-2.2	G190.9-2.2
G152.4-2.1	G152.4-2.1
G107.5-1.5	G107.5-1.5
G127.1+0.5	Monoceros
G205.5+0.5	G205.5+0.5
G347.3-00.5	G347.3-00.5
G180.0-1.7	S147
G260.4-3.4	Puppis A
G119.5+10.2	CTA 1
G327.6+14.5	SN 1006

Names are used in Fig. 1.

some classes, allowing their use as 'standard candles' (Hamuy and Pinto, 2002; Kasen and Woosley, 2009; Cano, 2014). The γ evolution in the first hours to several years after the explosion is known to vary also; in particular, some events fade and then re-emerge to produce large amounts of γ radiation months to several years after the initial explosion (Wang *et al.*, 2019*a*).

Many decades prior to any direct γ observations, SNe theory for core-collapse events already predicted prompt X- and γ radiation. Peak luminosities of 1.9×10^{45} erg s^{-1} were calculated, and the total hard γ energy from SNe was estimated to vary between 10^{47} and 10^{50} erg, radiated over a period of months (Colgate, 1975; Klein and Chevalier, 1978). Observational data for extragalactic objects later indicated that Type II SNe total explosion energies vary from 0.5 to 4.0×10^{51} erg (Kasen and Woosley, 2009). Perhaps an average of 0.01 of such energy is emitted as γ (Miyake *et al.*, 2012). Varying SNe γ emissions depend on the mass and type of the progenitor star, metallicity, rotation velocity, the type of event and whether a binary system was involved (Kann *et al.*, 2019).

Verified γ-emitting SNe now include: Type Ia white dwarf explosions (Churazov *et al.*, 2015), Type Ib, Ic and II massive star core-collapse events (Podsiadlowski, 2013), core-collapse hypernovae (Pian *et al.*, 2006), superluminous SNe (Moriya *et al.*, 2018), many or most long GRBs (Gehrels and Mészáros, 2012; Cano, 2014; Cano *et al.*, 2017) and subluminous long GRBs (Nakar and Sari, 2012). Prompt isotropic relativistic shock breakout γ emissions of 10^{48} and $10^{48–50}$ erg from 'standard' long GRBs (including those with beamed emissions) and also from subluminous GRBs are predicted by theory and agree with some observational data (Nakar and Sari, 2012). Intense γ emission over weeks to up to several years has now been observed from Type II SNe and can be sustained by shock-induced emission from a circumstellar medium (Wang *et al.*, 2019*a*). Finally, observations in the γ domain of the nearby core-collapse SN 1987 in the large Magellanic Cloud tested some of the relevant theory for γ in the months after the initial explosion (Matz *et al.*, 1988; Chevalier, 1992).

During a SN, an initial shock breakout may produce either beamed or isotropic γ emission or both (non-beamed emission may occur after the brief collimated burst). Observations with γ and X-ray observatories and optical telescopes demonstrate that many long (10–300 s) GRBs are a special class of extra-galactic, supermassive star SN with beamed γ emission reaching isotropic-equivalent energies of 10^{53} erg (Gehrels and Mészáros, 2012). At least one late Quaternary galactic SNR exhibits characteristics compatible with origin as a GRB (Lopez *et al.*, 2013). Also, XRFs (e.g. SN 2006j) produce prompt X-ray flashes. Such objects are half as luminous as some GRB-associated optical SNe; they attain total energies smaller than GRBs but greater than typical SNe, and may be isotropic radiators of both γ and X-rays (Pian *et al.*, 2006). Optically, some 'superluminous SNe' exhibit peak brightness approximately 10–100 times that of more common SNe (Moriya *et al.*, 2018). Their γ emissions may be larger as well; their precursor stars may be exceptionally massive. Some of the SNRs in Table 1 could represent events like these, though they are infrequent. Finally, for Type Ia (binary white dwarf) SNe, sometimes used as 'standard candles', observation of an extragalactic example indicates γ luminosities of $11 \pm 1 \times 10^{41}$ erg s^{-1} on day 73 and $6.5 \pm 0.6 \times 10^{41}$ erg s^{-1} on day 96 (Churazov *et al.*, 2015). A year of such emission would provide a total γ close to 10^{49} erg (depending on the size of the earliest emission).

Theory, modelling and observation using the orbital high-energy observatories are also helping constrain the time evolution of SNe γ emission. In part, the work is designed to facilitate early SNe detection. A significant fraction of the photon energy of a Type Ia SN emerges in hard X-rays and γ lines; total explosion energies exceed 10^{51} erg. The ejecta mass and expansion rate of Type Ia differ greatly from core-collapse SN, creating an early and strong signal in γ (Wang *et al.*, 2019*b*). Depending on models used, the peak γ flux occurs ∼60–90 days after explosion. For Type II events, γ depends on the level of the two-photon annihilation process (Cristofari *et al.*, 2020); multi-GeV and some TeV γ are expected in the first several days, followed by an interval of obscuration and no detection, and then re-emerging during a period of intense emission from ejecta–wind interaction (Wang *et al.*, 2019*a*). Hard γ is emitted as the shock wave interacts with soft photons from the SN photosphere through pair production, thereby temporarily suppressing the γ leaving the system. In the case of SN 1993J, γ attenuation was calculated at 10 orders of magnitude in the first few days after the SN explosion: γ would be detectible if observations are performed either earlier than 1 day, or later than 10 days after the explosion, when γ attenuation decreases to about 2 orders of magnitude (Cristofari *et al.*, 2020).

Total explosion energies, chemistry/spectra, masses and existence or absence of associated compact objects such as pulsars are obtained from SNR observations to constrain the probable precursor star characteristics and the size, type and physics of the explosion. Many GRBs and superluminous SNe may be hypernovae and produce black holes (Podsiadlowski, 2013): unusually energetic core-collapse SNe with supermassive star progenitors. Prompt emission in γ may be from successful or failed shock breakout (Nakar and Sari, 2010), some days prior to initiation of the optical event. Then, as the explosion evolves, γ radiation again emerges, and is sustained over a period of several years

https://doi.org/10.1017/S1473550420000348 Published online by Cambridge University Press

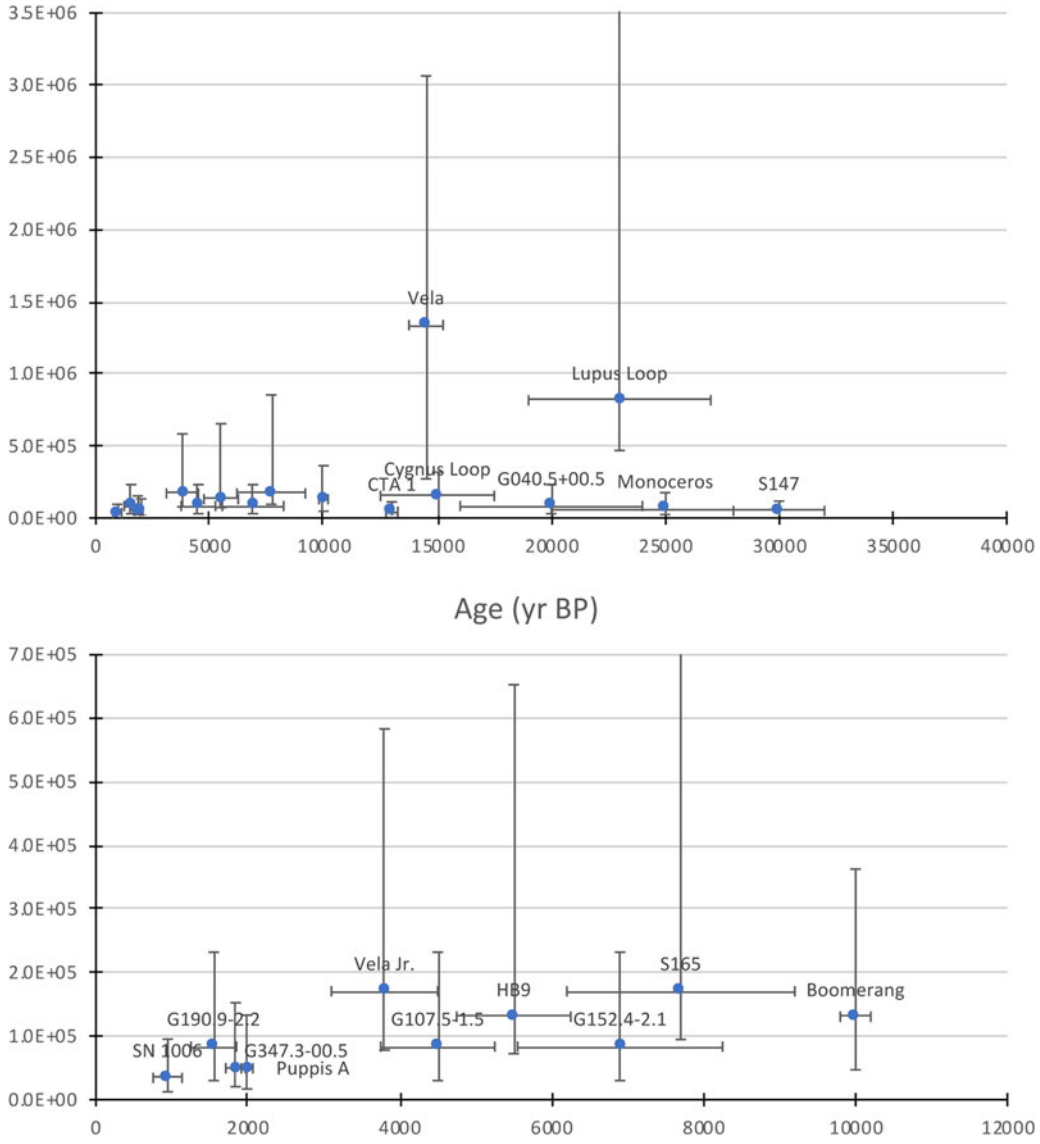


Fig. 1. Top: Intensity of SNe γ (total fluence incident on Earth) for 18 of the closest events. Bottom: Expanded view for the past 12 000 years. Data from Table 1, this paper. Ages are years before present (BP, before CE 1950).

dependent on characteristics of the expanding shell (Matz *et al.*, 1988).

The spectra for SN 1987A, the well-observed and relatively nearby core-collapse SN in the Large Magellanic Cloud, provides an example of sustained emission. Hard photon emission was observed between 0.02 and 2 MeV over 500 days; the measured total γ energy was 10^{46} erg (any initial emission was not monitored), and total SN energy was 1.4×10^{51} erg (Pinto and Woosley, 1988; Chevalier, 1992). However, the progenitor for 1987A was a blue supergiant with an initial mass of about 20 M⊙ instead of the more typical red supergiant, and the SN was fainter optically than typical Type II SNe at maximum by an order of magnitude (Chevalier, 1992).

Modelling of possible terrestrial γ effects from a more typical event (Gehrels *et al.*, 2003) used 10^{47} erg γ total, a spectral distribution binned into 66 logarithmic intervals 0.001–10 MeV, and a red supergiant progenitor of 15 M⊙. For comparison, the Vela X Y Z SN (Table 1) progenitor was 30 M⊙ (Sushch and Hnatyk, 2014). In the modelling, the Type II SN γ luminosity peaks at 340 days and is within a factor of 10 of the peak for 500 days. Also, γ emission in Gev energies has recently been observed in other Type II SNe and with a different evolution through time. Thus, between 0.2 and 500 GeV, over a 3 years emission time, the total energy released in γ-rays was 10^{51} erg, and the γ commenced 300 days after the explosion and lasted for another 850 days. This was a luminous but not particularly superluminous SN (Yuan *et al.*, 2018).

In summary, very large quantities of γ output from SNe were earlier predicted and are now firmly established from advanced modelling and direct observation. There is exceptional variability among the different classes of objects, and theory development is underway to explain the new data. Spectra have been obtained for SN objects from different classes and the flux trajectories, over timescales from seconds to several years, are increasingly being observed. This research allows an increasingly accurate evaluation of the implications for astrobiology. Some of the predicted terrestrial effects (e.g. on cosmogenic isotopes, atmospheric photochemistry and climate) will depend on the energy spectra

https://doi.org/10.1017/S1473550420000348 Published online by Cambridge University Press

and duration, but a total fluence estimate, even without such relevant information, remains useful (Table 1 and Fig. 1). At the temporal resolution of most terrestrial records (yearly to decadal, at best), the SN events are short, and it is the cumulative geochemical and geophysical results over each event that may be observable.

Potential solar system effects

The terrestrial effects of SNe radiation may include the interactions of γ at high energies with the upper atmosphere, Compton scattering creating a γ-initiated ionization cascade similar to cosmic ray protons and re-emission of γ at lower energies (including within the troposphere at energies where cosmogenic isotopes are generated), ionization of atmospheric gasses, and altered atmospheric and biological processes: as the energy is re-radiated (Scalo and Wheeler, 2002). Like particle cosmic rays, SNe hard photon effects on solar system planetary bodies are mediated by any atmosphere, which shields the surfaces, but absorbs, scatters and re-emits the radiation (Scalo and Wheeler, 2002; Pavlov *et al.*, 2013).

In this regard, relatively steady levels of radioactive ^{14}C are maintained in Earth's upper atmosphere by $^{14}N(n,p)^{14}C$ from incoming galactic and solar cosmic ray particles. However, γ photons from SNe can also produce ^{14}C, ^{10}Be and ^{36}Cl, ionize N by photonuclear reactions, and initiate neutron cascades (Lingenfelter and Ramaty, 1970; Damon *et al.*, 1995; Miyake *et al.*, 2012). Thermalized neutron yields from γ photons reach a maximum at about 23 MeV (from absorption around the giant dipole resonance for N and O nuclei), then rises again at MeV > 60 (Pavlov *et al.*, 2013). In contrast, ^{10}Be and ^{36}Cl maximum production could occur after additional progress of the energy through the atmosphere and γ emission at lower energies. Also, O^3, an important greenhouse gas and solar UV shield, may be depleted by the ionizing radiation, and catalytic reactions producing NO_x species initiated (Ruderman, 1974; Gehrels *et al.*, 2003; Thomas *et al.*, 2005).

The terrestrial ^{14}C record provides perhaps the best opportunity to test for SN effects. Since its development in the middle part of the last century, radiocarbon dating has proceeded based on the relatively constant production of ^{14}C in Earth's atmosphere by cosmic rays: as calibrated using ^{14}C assays on wood cellulose securely dated to actual year BP by dendrochronology (Stuiver, 1961). Radiocarbon production is, however, modulated by other factors, including the Earth's variable magnetic field and the Sun. There are short-lived 'wiggles' in the ^{14}C production rate and atmospheric concentration: most are attributed to solar cycle variations (Eastoe *et al.*, 2019). However: 'there are not many factors' that can induce abrupt elevations (sharp rises within 1–2 years) of ^{14}C (Pavlov *et al.*, 2013). Such rapid-increase anomalies in the Earth's atmospheric ^{14}C production have been observed in ^{14}C assays of individual tree ring records, although some actually extend over several years (Table 3). These are commonly attributed to (possibly) photon radiation from SNe or GRBs, or to cosmic ray particle radiation from exceptionally large solar flares or extended periods of high solar activity (Miyake *et al.*, 2012; Jull *et al.*, 2018). The viability of the first hypothesis is now further considered.

The historical CE 1006 example

Terrestrial radiocarbon production from SN γ in the 70 MeV to 10 GeV range is, in principle, measurable: for the historical SN 1006, if SN γ energies reach to 10^{50} erg (Damon *et al.*, 1995). Some prehistoric SN are much closer (Table 1). In order to constrain SNe γ requirements for ^{14}C production and its recording in terrestrial records, the relation between the observed ^{14}C changes (e.g. in tree ring wood), commonly expressed as $\Delta^{14}C$ (Stuiver and Polach, 1977), and ^{14}C production in the atmosphere must be modelled. Carbon cycle modelling, including the pathways of atmospheric ^{14}C and its incorporation into terrestrial records, is increasingly comprehensive (Kanu *et al.*, 2016). However, the purpose here is restricted to the identification of important candidate SNe that may have affected global production. Therefore, the published results of relatively simple four- or five-box models can be used to compare SN-predicted increases in ^{14}C production with observed biosphere $\Delta^{14}C$ changes (Table 1).

Note that, unlike particle cosmic radiation, Earth-incident γ is not affected by the geomagnetic field, and also that much of any SN ^{14}C (and several other cosmogenic isotopes) should be produced in the troposphere (Damon *et al.*, 1995). The complex atmospheric changes that may be initiated could also themselves affect the resulting ^{14}C record (Pavlov *et al.*, 2013): for example, how quickly ^{14}C is mixed between the northern and southern hemispheres, even under steady-state conditions, is still being investigated. As well, the tree ring chronologies themselves commonly exhibit regional offsets by <10 years, for reasons which may include dating/laboratory error but could also reflect actual regional differences whose causes are not yet understood (Pearson *et al.*, 2020).

The possibility of SNe affecting Earth's ^{14}C production has been investigated intermittently for several decades. Most of the relatively nearby objects in Table 1 have not been considered; instead, the historical SNe have been the focus (Damon *et al.*, 1995; Dee *et al.*, 2016). For example: in California tree ring records, a 5–9.5‰ $\Delta^{14}C$ rapid-increase tree ring anomaly commences at 942 BP and is followed by gradual decay over a decade (Tables 1 and 3). This is 2 years after the historic SN 1006

Table 3. Rapid ^{14}C increases (>7‰ $\Delta^{14}C$ rise within 5 years, decline to near the previous level within 20 years) so far identified by various workers from tree rings sampled at high resolution (2 years or higher)

Date (years BP)	‰ del 14C	Duration of rise (years)	Decay (years)	References
14 697	?	40	Not provided	Adolphia *et al.* (2017)
12 745	30	60	Not provided	Hua and Al (2009)
7431	20	10	Not provided	Miyake *et al.* (2017)
5372	9	1	10	Wang *et al.* (2017)
2610	12	6	10	Fahrni *et al.* (2020)
3478	8	6	6	Pearson *et al.* (2020)
2765	14	10	~100	Jull *et al.* (2018)
2615	13	3	10	Sakurai *et al.* (2020)
1176	12	2	10	Miyake *et al.* (2012)
957	10	1	10	Kudsk *et al.* (2019)
941	8	2	10	Eastoe *et al.* (2019)
941	5	2	10	Menjo *et al.* (2005)
941	9	2	10	Damon *et al.* (1995)

https://doi.org/10.1017/S1473550420000348 Published online by Cambridge University Press

(Lingenfelter and Ramaty, 1970; Damon *et al.*, 1995). For SN 1006, the authors used a distance of 1.3 kpc to calculate Earth-incident γ, and an intrinsic energy of 1×10^{49} erg in γ > 10 Mev. This produces 1.4×10^{4} erg cm^{-2} at Earth and yields approximately 650 thermalized neutrons per erg available to produce ^{14}C by ^{14}N(n,p)^{14}C (Lingenfelter and Ramaty, 1970). Thus, 0.9×10^{7} thermal neutrons generate the SN-related ^{14}C (Damon *et al.*, 1995). If this arrives in 1 year, the ^{14}C production is 0.3 a cm^{-2} s^{-1}, as compared to the annual steady-state production by cosmic rays of 1.64 a cm^{-2} s^{-1} (Kovaltsov *et al.*, 2013).

The observed tree ring anomaly, which decays over 9 years, was fit via carbon cycle box modelling to a 1 year only, 2.5× increased ^{14}C production rate (Damon *et al.*, 1995). A subsequent tree ring search for the same ^{14}C anomaly from another geographic location (Japan) was successful; a +5‰ Δ^{14}C increase was measured, which is more compatible with causation from this relatively distant SN (Menjo *et al.*, 2005): the predicted effect on ^{14}C is small. Although this result was not replicated at a location in England (Dee *et al.*, 2016), recent remeasurements of the California wood verify the earlier results; also other, smaller (<5‰) positive (step-wise) anomalies were observed at CE 1063, 1167, 1297, 1429 and 1448–1450 (Eastoe *et al.*, 2019).

The distance of the SN 1006 SNR (G327.6+14.5, pulsar PKS 1459-41) has since been revised to 1.56 kpc (Jiang and Zhao, 2007). Also, a lower, 20–55 a erg^{-1} mean yield (adjusted to a spherical Earth target) is used by Pavlov *et al.* (2013) for γ entering the atmosphere from a hypothetical GRB with typical spectral parameters. Other recent studies use a production rate of 130 a erg^{-1} (Usoskin *et al.*, 2013) for γ-related production, once divided by 4 this is ~32 a erg^{-1}. This value is used in Table 1 for all events for uniform comparison purposes. For SN 1006, using a 4×10^{49} γ energy, the 130 a erg^{-1} production rate, the reduction by ¼ to adjust to a spherical Earth and the revised distance, the predicted changes in ^{14}C again produce a small anomaly for SN 1006 (Table 1). The calculated extra production of 0.1–0.3 a cm^{-2} s^{-1} is still much less than the modelled need for 2.1 a cm^{-2} s^{-1} for the 9‰ Δ^{14}C, and also less than that needed for the 5‰ Δ^{14}C increase measured at the second site (Wang *et al.*, 2020). Damon *et al.* (1995) address this problem by inferring that the SN must have emitted 10^{50} erg in γ, which does fall within the known range of variability in SN γ emissions (see above).

In regard to the slightly lagged response of tree ring ^{14}C to this historic SNe, ring-based ^{14}C concentrations reflect tropospheric conditions during wood formation, and some time lag is expected; such lags are variously accommodated by different box models (Pavlov *et al.*, 2013). However, the lag, in this case, is also in agreement with a new understanding about the potential duration of SN γ emission. SN 1006 is considered to be a Type 1a white dwarf event, which re-brightened (Jiang and Zhao, 2007); not all of the relevant γ was likely to have been produced in 1 year. The observed ^{14}C anomalies at 942 BP, 2 years later (Damon *et al.*, 1995; Menjo *et al.*, 2005), fit what is now known about the probable evolution of γ radiation from an SN of this type.

Comparison of prehistoric SNe γ to the ^{14}C record

At a distance of 1.56 kpc, SN 1006 is more distant than many other known SNe during late Quaternary time. Previous examinations of the capability of SNe to affect Earth's atmosphere have mainly focused on the historical SNe; none of these were exceptionally close to the Earth. However, there are 18 SNe with distance estimates ≤1.5 kpc and ages less than 5×10^{4} BP (Table 1, Fig. 1). One is as close as ~0.25 kpc.

The IntCal13 (Reimer, 2013) and separately reported records with much better temporal resolution can be used to examine the case for predicted effects. Dendrochronologically-dated tree rings provide the assayed carbon for the younger, <12 500 BP, part of IntCal13. Other materials sample ^{14}C in the upper mixed ocean (marine corals and foraminifera), soil water (speleothems) or lake biota (Southon *et al.*, 2012). The complete IntCal13 temporal coverage is 50 000 BP to present, with much loss of temporal resolution and attenuation of any brief pulses of atmospheric ^{14}C in the older part of coverage. Thus, the temporal sampling is 20 years from 26 000 to 15 020 BP, 10 years from 15 000 to 12 500 BP, and 5 years from 12 495 to 0 BP (Reimer, 2013). IntCal13 may not detect short-term variations lasting less than 500 years earlier than 15 000 BP at all, unless they are exceptionally large. IntCal13 smooths and attenuates any abrupt changes, even if global, and even in the youngest portions of its coverage. It is used here only for a common comparison of different possible events and more detailed information is provided where available.

With these constraints, the closest eight late Quaternary SNe are evaluated individually, in order of distance, compared to the ^{14}C record (see also Tables 1 and 3). The more temporally detailed assays are also used. The ages provided for each event are those of the initiation of the ^{14}C anomaly and are in calendar years BP. The SNR's catalogue number and name are in each case paired with the possible ^{14}C anomaly, by age.

Example 1: G263.9-03.3, Vela X Y Z and 12 740 BP

The nearest of late Quaternary SNe, the older Vela SN core collapse of a 30 M⊙ star occurred (within uncertainty) at the same time as a large and sudden positive global ^{14}C anomaly in the IntCal13 record (Tables 1 and 3, Fig. 2(a)). Vela's distance of 0.25 ± 0.03 kpc is from Ca II absorption line spectra (Cha *et al.*, 1999) and there is an independent distance estimate of 0.29 + 0.019, −0.017 kpc from VLBI parallax measurements on the associated pulsar (Dodson *et al.*, 2003). Caraveo *et al.* (2011) also obtain a distance of 0.29 + 0.076, −0.050 kpc from Hubble parallax measurements. The age is estimated as 14 500 ± 1500 years from shock velocity considerations (Wallerstein and Silk, 1971; Cha *et al.*, 1999); the pulsar characteristic age is 11 400 years (these are commonly considered minimum ages). The hydrodynamical age from modelling of the radio SNR is 7000–12 000 years (Sushch and Hnatyk, 2014). Vela's proximity indicates that a ^{14}C isotope signal should be detectible.

In floating chronology tree ring records with close-interval sampling, a +30‰ Δ^{14}C increase occurs within 60 years starting at 12 740 BP, and reaches +45‰ after another 40 years (Hua and Al, 2009) (their Fig. 7; not illustrated here). The (smoothed) IntCal13 curve instead provides a +25.3‰ Δ^{14}C from 12 745 to 12 640 BP and increasing another 5.4‰ to 12 515 BP (Fig. 1(a)). These latter results are based on decadal samples. Carbon cycle considerations and lags in cross-hemisphere atmospheric mixing suggest that several years would be required for full incorporation of the pulse into the global atmosphere and thence into ^{14}C-recording materials such as tree rings. Also, for a nearby event, the predicted sustained emission several years after the explosion may be significant. After any sharp increase, a decay period is expected as the excess ^{14}C is assimilated and merges with the normal annual production values for that time interval.

https://doi.org/10.1017/S1473550420000348 Published online by Cambridge University Press

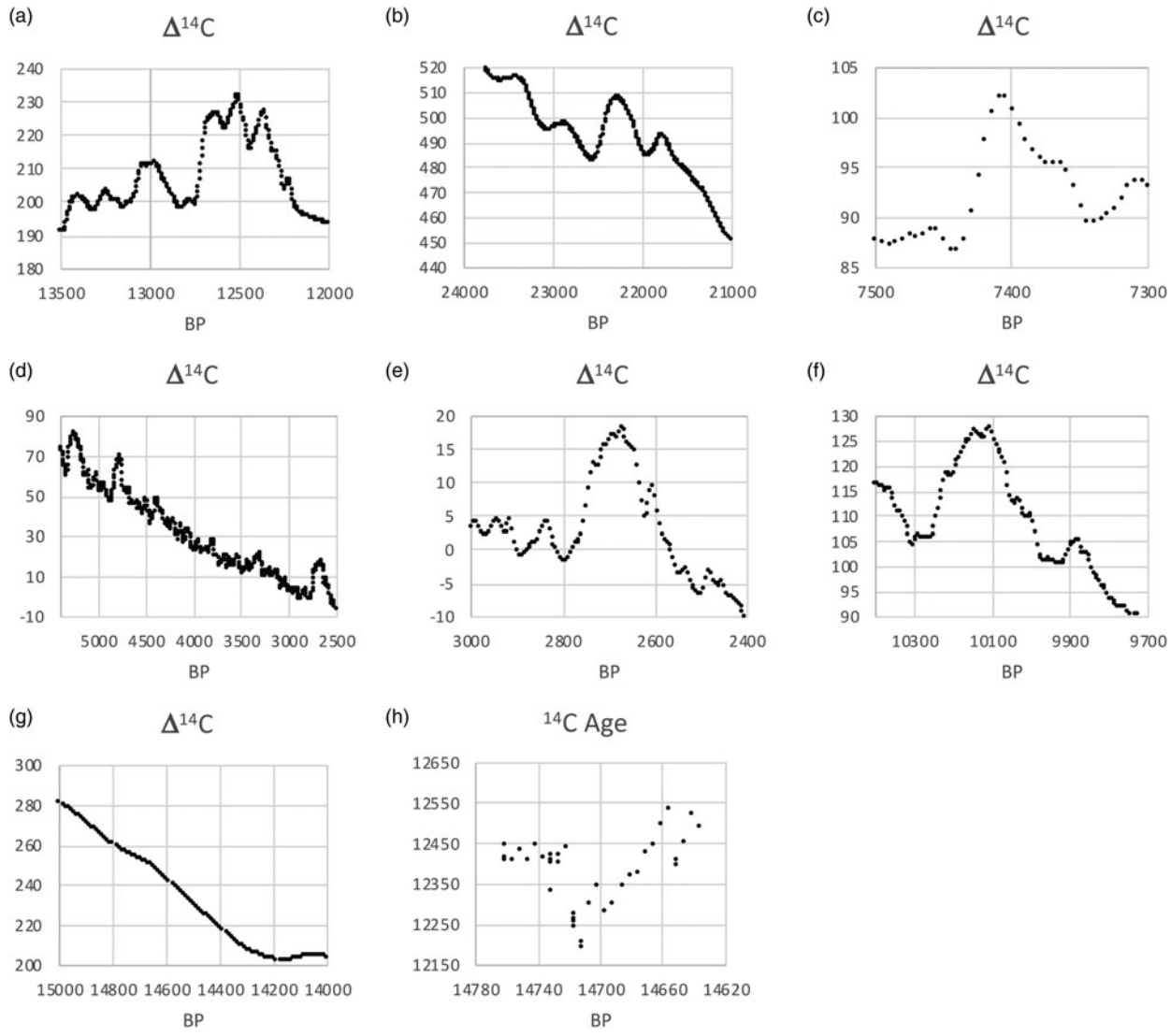


Fig. 2. Radiocarbon variation at the times of nearby prehistoric SNe. (a) A steep 25.3‰ rise in $\Delta^{14}C$ occurs in IntCal13 at 12 745–12 640 BP. (b) A 21‰ IntCal13 $\Delta^{14}C$ rise occurs at 22 500 BP, but the coarse temporal resolution is inadequate to reveal brief anomalies. (c) IntCal13 shows a steep rise in $\Delta^{14}C$ of 15.3‰ at 7440–7410 BP. Single-year tree ring data show a 20‰ rise from 7431 to 7421 (Miyake *et al.*, 2017). (d) At least three rapid-increase ^{14}C anomalies may be illustrated in this IntCal13 plot spanning 5500–2500 BP: one at 5340 BP, one at 4880 BP and one at 2765 BP. (e) At 2765–2735 BP, $\Delta^{14}C$ rises by 11.4‰ in 30 years, at the approximate time of the Vela Jr. SN. (f) Between 10 255 and 10 220 BP, $\Delta^{14}C$ rises by 12.2‰ at the approximate time of the Boomerang SN. (g) IntCal13 data for 15 000–13 000 are without detailed time resolution and can reveal no short-lived anomalies. (h) Floating tree-ring chronologies with closer temporal sampling, however, document a strong and short-lived $\Delta^{14}C$ increase marked by younger radiocarbon dates just after 14 697 BP (Adolphia *et al.*, 2017) and compatible with the age and probable γ intensity of the Cygnus Loop SNR.

The timing of the $\Delta^{14}C$ increase is synchronous with abrupt terrestrial climatic changes at the onset of the Younger Dryas Stadial: an interval of sharply cooler temperatures, especially at temperate to high northern latitudes (Hughen *et al.*, 2000). However, a system-internal mechanism has been suggested for the Younger Dryas increase: temporary cessation of North Atlantic Ocean deep/shallow water circulation, which can possibly explain the elevated ^{14}C. However, then a triggering cause must still be located (Siegenthaler *et al.*, 1980). The rapid changes starting at this time agree with predictive modelling of cooler temperatures and other atmospheric changes possibly caused by a γ radiation event (Thomas *et al.*, 2005). Thus, sharply increased NO_x-induced atmospheric opacity and reduction of O_3, which is an important greenhouse gas, both favour cooler temperatures. These are numerically modelled to occur if the results of Melott *et al.* (2005) are applied: the 10^8 erg of GRB kev γ at a distance of 2 kpc used for modelling by Melott for a major extinction-causing GRB (at the end of the Ordovician Period) is 6.4×10^7 erg for the 8× closer, non-GRB (4×10^{49} erg) Vela, and thus comparable to the predicted 1.1–1.7×10^6 erg for this actual SN (Table 1). As well, a major mammalian extinction did occur at the start of the Younger Dryas (Barnosky *et al.*, 2004; Faith and Surovell, 2009; Brakenridge, 2011).

Causation of the steep rise of ^{14}C at the start of the Younger Dryas remains controversial (Olivier *et al.*, 2001); a variety of Earth system-internal changes occurred then, and oceanic circulation can clearly affect atmospheric ^{14}C concentrations. However, the very rapid and large ^{14}C increase, observed in both tree rings and varved marine sediments (Hughen *et al.*, 2000), has

https://doi.org/10.1017/S1473550420000348 Published online by Cambridge University Press

remained difficult to explain or model with only changes in oceanic circulation. From Renssen *et al.* (2000):

> 'The second feature in the Cariaco basin $\Delta^{14}C$ record not replicated by our model is the rapidity of the $\Delta^{4}C$ increase at the onset of the Younger Dryas…If the rapid $\Delta^{14}C$ increase at the onset of the Younger Dryas observed in the Cariaco basin record is a faithful reflection of a $\Delta^{14}C$ change in the atmosphere at that time, the previous concern to explain the early $\Delta^{14}C$ drawdown during the Younger Dryas should be substituted by a new concern to explain this increase.'

The SN-predicted increased global production of ^{14}C, 4.4–7.1 a cm^{-2} s^{-1}, is much higher than the average steady-state value of 1.64 a cm^{-2} s^{-1} from cosmic rays. Also, this was an exceptional Type II SN event, with a high precursor mass and a total explosion energy of 1.4×10^{51} erg (Sushch and Hnatyk, 2014). The timing, proximity and energy of this prehistoric SN, when compared to the rapid increase, size, global extent and timing of the ^{14}C anomaly, support a possible cause and effect relationship. If indeed climate was affected, at a time of continental deglaciation, then Earth system-internal changes, already underway, may also have been affected, and further perturbed the carbon cycle.

Example 2: G330.0+15.0, Lupus Loop and 22 500 BP

This SNR may be, within large uncertainty limits, nearly as close (0.32 kpc) as Vela X Y Z, but it is older and also of uncertain age: 23 000 ± 8000 BP (Table 1, Fig. 1) (Safi-Harb *et al.*, 2012). The possible, though uncertain, proximity merits discussion here of its potential terrestrial effect.

In the IntCal13 record, greatly smoothed for this time period, there is a relatively steep 21‰ $\Delta^{14}C$ increase over 140 years at 22 500 BP (Fig. 1(b)). Unlike the case for Vela, there is no close-interval ^{14}C sampling available. A revised Σ–D relation estimates the SNR distance at 0.5 kpc (Pavlovic *et al.*, 2014); an age of 50 000 BP may also be consistent with the X-ray observations. Without more narrow SN age constraints and without detailed ^{14}C sampling, no confirmation or falsification of the predicted (Table 1) ^{14}C effects from this SN is possible. The smoothed Intcal13 data in Fig. 2(b) are, however, compatible with an SN signal of the expected size and at an appropriate time. Modulation by geomagnetic or solar activity changes is also possible because the changes may in reality indeed be as gradual as indicated in IntCal13.

Example 3: G114.3+00.3, S165 and 7431 BP

IntCal13 results show a steep rise of 15.3‰ $\Delta^{14}C$ between 7440 and 7410 BP and are provided in Fig. 2(c), but detailed ^{14}C assays for this period from Bristlecone Pine are also available with a 1–2 years resolution. They demonstrate a large increase (20‰) over 10 years, from 7431 to 7421 BP (Miyake *et al.*, 2017). Recently, the distance of S165 was revised downward to ∼0.7 kpc and with an age of approximately 7700 years. The total energy is unusually high and estimated at 5×10^{51} erg as a Type II event (Yar-Uyaniker *et al.*, 2004). The distance is from associated patches of H I and H II emission (Safi-Harb *et al.*, 2012), and there is also a central pulsar.

The rapid rise, magnitude and duration of the ^{14}C anomaly is compatible with causation by this close and potentially powerful SN γ source. However, abnormal solar activity has instead been invoked (Miyake *et al.*, 2017; Jull *et al.*, 2018). Yet, S165 appears to be of appropriate age and distance to be associated with this terrestrial ^{14}C anomaly. The estimated S165 elevation of the ^{14}C production rate over 1 year is 0.3–2.8 a cm^{-2} s^{-1} (range due to the distance uncertainty), whereas box modelling and comparison to solar modulation effects of the ^{14}C anomaly indicate a total ^{14}C increase in production between 6.0 ± 2.4 and 10.5 ± 3.0 a cm^{-2} s^{-1} (Miyake *et al.*, 2017). Predicted SN effects are significant compared to annual steady-state production, and should be detectible, but they are smaller than what the tree-ring assays and carbon cycle modelling indicate is required. Modelling has, however, not yet been performed to evaluate a ∼3–4 years long receipt of SN γ, as compared to a single solar superflare or a prolonged period of higher solar activity (Miyake *et al.*, 2017). Also, as noted, the emitted energy was likely higher than used in Table 1. SN causation for the observed anomaly is viable, given that a relatively nearby and high-energy candidate SN has been identified, and that its emissions may have been intense and prolonged over several years.

Example 4: G266.2-1.2, Vela Jr. and 2765 BP

The IntCal13 radiocarbon chronology shows a $\Delta^{14}C$ rise of 20‰ (Fig. 2(d) and (e)) at 2765 BP. This anomaly has recently been further investigated by more detailed tree ring ^{14}C data demonstrating a rapid rise of approximately 13‰ at 2765–2749 BP (Jull *et al.*, 2018). Vela Jr. is a shell-type SNR in the same line of sight as G263.9-03.3 Vela X Y Z. Its age is estimated at 3800 ± 1400 years and distance at 0.75 ± 0.25 kpc (Allen *et al.*, 2015). No associated pulsar or other compact object has so far been observed: this may indicate a supermassive star precursor.

The SN age is between 2400 and 5100 years if it is expanding into a uniform ambient medium; if it is instead expanding into the material shed by a steady stellar wind, then the age may be as much as 50% older. Thus, SN causation for the brief, rapid-increase ^{14}C anomaly at 2765 BP is plausible, but without a tighter age constraint (Table 1, Fig. 1), the correlation in time is not secure. The ^{14}C anomaly exhibits a relatively slow rise (10 years) (Table 3): compatible with Vela Jr. if it was accompanied by extended γ emission, but other causation is inferred (Jull *et al.*, 2020). Vela Jr., given its probable energy and proximity, likely did leave a trace in the terrestrial ^{14}C record; better understanding of its age can test the possible specific connection to ^{14}C changes.

Example 5: G160.9+02.6, HB9 and 5340 BP

IntCal13 results indicate a +18‰ ^{14}C anomaly commencing at 5340 BP (Table 1 and Fig. 2(d)), but a rise that is not as steep as others, to ∼5280 BP. However, a detailed tree ring study (Wang *et al.*, 2017) concludes an abrupt rise (+9‰ in 1 year) in 5372 BP with a decay period of about 10 years. This result, from a floating tree ring chronology and buried logs, has not been validated by other workers (Jull *et al.*, 2020; Wang *et al.*, 2020); a dating error may be involved. HB9 is a radio SNR with an associated magnetar/pulsar compact object. The age is estimated at 4000–7000 BP based on the Sedov equation and evaporative cloud modelling (Leahy and Tian, 2007). It is nearly as close as Vela Jr., at 0.80 ± 0.40 kpc. HB9 may be of appropriate distance and age to be compatible with this brief ^{14}C anomaly; its emission energy was also likely to have been unusually high.

Example 6: G106.3+02.7, Boomerang and 10 255 BP

At this time, a 12‰ rise in $\Delta^{14}C$ occurs within 35 years in the IntCal13 results (Fig. 2(f)). The steep rise is followed by a more gradual but sustained rise to 10 145 BP (another 10‰), possibly of different causation. The Boomerang SNR is ∼10 000 years in

https://doi.org/10.1017/S1473550420000348 Published online by Cambridge University Press

age and is at a distance of ~0.8 kpc. Table 1 provides another SN, G89.0+4.7, with an appropriate age (9900 ± 5100 BP) but at a greater distance (1.25 ± 0.45 kpc). The larger distance implies a significantly smaller ^{14}C effect. The Boomerang SN is more consistent with the measured anomaly at 10 255 BP (Table 1). Single-year tree ring analysis is needed to further constrain the characteristics of ^{14}C through this time interval. As the case for the Lupus Loop example, the data presented here are compatible with SN causation, but better age and distance estimates for the SN are needed.

Example 7: G107.5-1.5 and 4880 BP

The IntCal13 record includes a brief, positive (17.6‰ rise in $\Delta^{14}C$) anomaly at 4880–4820 BP (Fig. 2(d)), but the existence of an appropriate rapid-rise anomaly cannot be determined from these data. However, the G107.5-1.5 SN is also close to the Earth, at 1.1 kpc, and may be of appropriate age: 4500 ± 1500 (Kothes, 2003). As for Boomerang and Lupus Loop, single-year tree ring analysis is needed to further constrain the characteristics of ^{14}C through this time interval.

Example 8: G074.0-08.5, Cygnus Loop and 14 722 BP

The IntCal13 record bracketing this time reveals no brief anomalies (Fig. 2(g)), but floating tree ring records document a relatively brief episode of much-increased atmospheric ^{14}C concentration (Adolphia *et al.*, 2017) (compare Fig. 2(g) and (h)). The Hulu Cave speleothem data from China also support a brief (10 years) atmospheric ^{14}C excursion (Southon *et al.*, 2012). The $\Delta^{14}C$ increase occurs at the beginning of another short-lived but geographically extensive cold interval in climate history: the Older Dryas Stadial (Mangerud *et al.*, 2017). The Cygnus Loop exhibits a radio and X-ray shell (Fesen *et al.*, 2018*a*) and its distance is now constrained to 0.74 ± 0.03 kpc (Fesen *et al.*, 2018*b*). If the true SN age is close to 15 000 BP, then the Cygnus Loop SN may have caused the brief but significant 14 722 years BP ^{14}C anomaly (Table 1).

More recent SNe events

The other SNe listed in Table 1 are at distances of approximately 1–1.4 kpc, with the addition of the unusually bright SN 1006 at 1.6 kpc (for which a possible ^{14}C signal has been recorded). These more-distant SNe may also be detectable by ^{14}C assays with yearly temporal resolution if the γ emitted was sufficiently energetic. In this regard, two rapid-increase, global and short-lived ^{14}C anomalies have been identified at 1176–1175 BP (CE 774–775) and 957–956 BP (CE 993–994) in single-ring tree ring assays (Miyake *et al.*, 2012; Miyake *et al.*, 2013; Table 3). New data covering the CE 966–1057 period suggest that the increase in atmospheric ^{14}C previously associated with CE 994 actually occurred in CE 993 (Kudsk *et al.*, 2019) and this date is provided in Tables 1 and 3.

The shapes of the ^{14}C time series for both events are similar: rapid increase within 1–2 years followed by a decade-long decay that could reflect dampening from the operation of the carbon cycle (Table 3). The magnitude of the younger ^{14}C event is 0.6 of the older, suggesting, if intrinsic energies of associated SNe were similar, that the younger SN was ~1.3× more distant. Plausible candidate SNe would be *G347.3-00.5* at 1.3 ± 0.4 kpc and approximately 1840 ± 260 years in age (Tsuji and Uchiyama, 2016), and the recently discovered and elongated *G190.9-2.2* at 1.0 ± 0.3 kpc (Foster *et al.*, 2013) (Table 1). Both are significantly closer than SN 1006 at ~1.56 kpc.

The ~1 kpc distant *G190.9-2.2* remnant is of a similar mean radius and thus age as W49B: an SNR at 8 kpc distance that may record a GRB (Lopez *et al.*, 2013). That event is described by Pavlov *et al.* (2013) as having possibly produced the 1176 years BP ^{14}C anomaly. For G190.9-2, and using the 130/4 ^{14}C a erg^{-1} production rate, a d = 1 kpc SN release of 4×10^{49} erg of γ causes a 1 year addition of 0.2–0.6 a cm^{-2} s^{-1} (Table 1), whereas box modelling of the needed additional ^{14}C indicates 3.9 a cm^{-2} s^{-1} (Miyake *et al.*, 2013, Pavlov *et al.*, 2013, Usoskin *et al.*, 2013). If this SN was as close as 0.7 kpc and emitted somewhat more energy, then the predicted ^{14}C production reaches to that estimated by the carbon cycle modelling and the tree ring data. Although SNe causation was ruled out by Pavlov *et al.* (2013) because no apparent candidate SNR then existed, the SNR was newly reported and analysed the same year (Foster *et al.*, 2013).

The *G190.9-2.2* SNR, like W49b, lacks a pulsar central object, is elongated, and its shape suggests the development of very energetic shock breakout γ accompanying a failed jet; or it may have resembled the SN1987A event. In either case, it appears that this recently discovered SN may be a stronger candidate than W49B as an emitter of radiation sufficient to cause the ^{14}C anomaly. Also, a possible historical sighting occurred in CE 774: a 'red cross in the sky' in the Anglo-Saxon Chronicle (Allen, 2012; Lovett, 2012). This is compatible with the SN's location in the northern hemisphere sky, and a new, bright, non-point source optical object agrees with the observed complex-ringed appearance of the expanding SN1987A remnant, in early stages of its evolution (Chevalier, 1992). A bright auroral display is not recorded, although they are reported in other years near this date (Stephenson, 2015). This recently discovered nearby SNR provides independent evidence of a bright SN at an appropriate time. It may also be compatible with ice core ^{10}Be records through this time interval that are considered by others to be caused by an SEP (Sukhodolov *et al.*, 2017). Modelling (Pavlov *et al.*, 2013) indicates a higher production of ^{14}C than ^{10}Be from incoming SN γ if it is mainly in the Mev range; but this differential does not rule out significant ^{10}Be generation.

G347.3-00.5 (Table 1) is a possible candidate for causation of the somewhat less intense CE 993 tree ring ^{14}C anomaly. It also was a close SN, very energetic at 10^{51} erg (Tsuji and Uchiyama, 2016), and its age may be compatible with the anomaly date, given the uncertainties with distances and ages. In this regard, however, instead of any visible SN-like object, a survey of historical records from Ireland, Germany and Korea show several reports of possible auroral activity commencing on 26 December 992. For example, 'On the night of the birth of St. Stephan, at the first cockcrow, light like the Sun shone from the North and many people said the Sun had risen. This continued for a whole hour. Afterwards, the sky was slightly reddened and returned to the normal color'. Similar but less detailed records occur from Ireland and Germany. These are compatible with the occurrence of 'intense solar activity' and a solar particle event at this time (Hayakawa *et al.*, 2017).

These accounts may as well be compatible with SN causation. The location of *G347.3*-00.5 in Scorpius indicates that the SN would not have been visible at night from northern latitudes in winter except shortly before dawn. Its position was also considered incompatible with Chinese records of a possible SN at CE 393 (Fesen *et al.*, 2011); that association has been largely ruled out. Also, not only solar particle events can affect the Earth's

https://doi.org/10.1017/S1473550420000348 Published online by Cambridge University Press

ionosphere and excite red glow-producing O_2 energy transitions. On 27 December 2004, a giant γ-ray flare from SGR 1806-20 (a magnetar; a special class of neutron star) at 12–15 kpc distance created a massive disturbance in the Earth's daytime lower ionosphere. The radiation (~380 s) dramatically increased ionization in the lower ionosphere down to ~20 km altitude for >1 h (Inan *et al.*, 2007) and an X-ray afterglow occurred for 16 h. A γ-emitting SN in earliest CE 993 may have produced even stronger (and visible) upper atmospheric effects, including short-lived but major optical emissions from Compton scattering: creating a γ-initiated ionization cascade similar to cosmic ray protons (Scalo and Wheeler, 2002).

As the case for CE 774, it is premature to rule out SN causation of this ^{14}C anomaly. The advantage of the SN hypothesis for both events is that the exceptionally energetic SNe certainly did occur and at approximately the right times. The disadvantage is that it is not yet possible to more tightly constrain their ages and the γ radiation and energy cross-sections received at Earth. In any case, it appears very likely that both rare and very energetic solar particle events and also significant SNe γ events affected the Earth during the past 40 000 years.

Discussion and conclusions

Changes in atmospheric cosmogenic isotope abundance on Earth can be used to monitor the exposure of the Earth and the rest of the solar system to high-intensity radiation events: from SNe, or from solar 'super-flares' or coronal mass ejection events. Determining actual causation is relevant to the knowledge of the Earth's radiation history, to the search for life within our own and in other solar systems, and to human space exploration. Yet the physical origins of the rapid-onset ^{14}C anomalies, a type of evidence that appears to monitor radiation events, still remain uncertain (Wang *et al.*, 2020). Contrary to Usoskin *et al.* (2013) and Dee *et al.* (2016), the evidence presented here clearly indicates that SNe radiation events may have had a significant impact during the past 40 000 years.

This paper presents eight candidate SNe, and, in particular, four events where one or more of the predicted effects occur at the correct time on Earth. These are: Vela, at 12 740 years BP; S165 at 7431 BP; Vela Jr. at 2765 BP; and HB9 at 5340 BP. Their ages, distance and expected γ emissions are compatible with observed terrestrial effects that are also predicted from theory and modelling, and with the increasingly abundant and detailed observations of γ from extra-galactic SNe. However, given the variety of SNe objects and their associated released γ radiation, the distances only partly determine the expected terrestrial ^{14}C signals. In this regard, however, the relative sizes of the ^{14}C anomalies do generally agree with a causal connection: the closer SN events are broadly associated with the larger observed isotopic changes (Table 1).

There are significant differences in how three cosmogenic isotopes, ^{14}C, ^{10}Be and ^{36}Cl, may respond to the two types of causality, and some workers have concluded, for particular events, that strong responses for all three favour a particle event. However, Sigl *et al.* (2015) found timing differences between the peaks, and Mekhaldi *et al.* (2015) adjusted ^{10}Be and ^{36}Cl ice-core records to match tree ring ^{14}C peaks in timing, under the assumption that they were responses to the same event (Wang *et al.*, 2020). Such data cannot, therefore, yet be used to falsify SNe causation. The ^{10}Be and ^{36}C ice core results also lack the exceptionally tight temporal control needed for an unbiased comparison at these timescales (Wang *et al.*, 2020). Finally, from incoming γ energy, enhanced production of all three isotopes can occur as the incoming radiation penetrates the upper atmosphere and is re-emitted at energies relevant to their production (Damon *et al.*, 1995; Scalo and Wheeler, 2002).

There is a reasonable expectation that both SNe radiation events and very large solar flares (or SEPs) have occurred in Earth history. Thus, in the yearly ^{10}Be data covering the last 400 years, there are significant anomalies at about CE 1460, 1605, 1865 and 1890 in the North Greenland Ice Core Project (Wang *et al.*, 2020); all are unrelated to strong ^{14}C variations but may record flares. Whether the Sun can produce the very large particle events needed to produce the tree ring-recorded changes is still debated: Neuhäuser and Hambaryan (2014) calculated the probability for one solar super-flare with energy larger than 10^{35} erg within 3000 years to be as low as 0.3–0.008. However, surveys of other solar-type stars indicate they may be possible (Dee *et al.*, 2016). The inventory of possible SNe and terrestrial record linkages presented here provides additional information and can facilitate further testing of the utility of both hypotheses.

There are several approaches that could be employed in such additional work. These include:

(1) Statistical tests of the correlation in time of the SNe and the proposed matching ^{14}C anomalies (perhaps limited to the past 14 000 years, where standard errors are the lowest);
(2) Quantitative examination of the 'dose-response' relationship, to identify the extent to which, assuming constant intrinsic γ emissions, the nearer SNe indeed caused stronger terrestrial isotope response;
(3) Further astrophysical observational and modelling studies focused on individual SNR ages, distances, type of event, and observed total and expected γ energies;
(4) Further observations and modelling of extragalactic SNe using the high-energy satellite observatories, in order to better constrain the γ energy cross-sections and durations of 'typical' SNe of various types;
(5) Modelling of the atmospheric ionization cascades initiated by the γ emissions, to better constrain predicted line emissions for high-energy photons corresponding to ^{14}C, ^{10}Be and ^{36}Cl production;
(6) Investigations using terrestrial geologic and paleoecological records of the other climate and atmospheric chemistry effects predicted, and especially for the nearest of the surveyed SNe.

In conclusion, the presented data and analysis do not rule out solar flare or solar activity hypotheses (Usoskin *et al.*, 2013; Jull *et al.*, 2018; Scifo *et al.*, 2019) for rapid-onset ^{14}C increases. However, SNe causation instead is viable for many of them. SN γ energies adequate to have produced the ^{14}C pulses were much earlier predicted from theory; they have now been directly observed for SNe outside of our Galaxy. The nearest in-galaxy events recorded by SNRs appear to have left traces in terrestrial isotopic and other paleoenvironmental records at the appropriate times and of the predicted relative magnitudes. The very nearest SNe, in particular, are the strongest candidates: for example, the older Vela SN, at ~0.25 kpc, with relatively tight age and distance constraints, a very massive precursor star and a steep rise in ^{14}C at the appropriate time. If SNe causation of the cosmogenic isotope changes did not, however, occur, then the detailed isotopic records now being produced, from tree rings, ice cores, speleothems and other sources, may indeed provide information only about intense flares of solar cosmic radiation (Miyake

https://doi.org/10.1017/S1473550420000348 Published online by Cambridge University Press

et al., 2017) and/or other environmental changes. If SNe instead caused some or all of these events, then part of the solar system radiation hazard to life is from hard photons from nearby SNe, and some events may have produced recorded paleoecological changes. In this case, the hazard to life is susceptible to further testing and quantification by investigation of the array of specific SNe events that are known to have occurred within our Galaxy and relatively near the solar system.

Acknowledgement. All data sources are provided in the references cited. D. Green, R. Sternberg, M. Sorensen, M. Willmes and five anonymous reviewers provided useful comments on earlier versions of this paper. The work was partially supported by faculty research funds provided by the University of Colorado.

References

Adolphia F, Muscheler R, Friedrich M, Güttlere L, Talamo S and Kromerc B (2017) Radiocarbon calibration uncertainties during the last deglaciation: insights from new floating tree-ring chronologies. *Quaternary Science Reviews* **170**, 98–108.

Allen J (2012) Astronomy: clue to an ancient cosmic-ray event?. *Nature* **486**, 473.

Allen GE, Chow K, Delaney T, Filipović MD, Houck JC, Pannuti TG and Stage MD (2015) On the expansion rate, age, and distance of the supernova remnant G266.2-1.2 (Vela Jr.). *The Astronomical Journal* **798**, 12 pp.

Barnosky AD, Koch PL, Faranec RS, Wing SL and Shabel AB (2004) Assessing the causes of Late Pleistocene extinctions on the continents. *Science* **306**, 70–75.

Brakenridge GR (1981) Terrestrial paleoenvironmental effects of a late quaternary-age supernova. *Icarus* **46**, 81–93.

Brakenridge GR (2011) Core-collapse supernovae and the Younger Dryas/terminal Rancholabrean extinctions. *Icarus* **215**, 101–106.

Cano Z (2014) Gamma-ray burst supernovae as standardizable candles. *The Astrophysical Journal* **794**, 9.

Cano Z, Wang S-Q, Dai Z-G and Wu X-F (2017) The observer's guide to the gamma-ray burst supernova connection. *Advances in Astronomy* **2017**, 41.

Caraveo PA, De Luca A, Mignani RP and Bignami GF (2011) The distance to the vela pulsar gauged with Hubble space telescope parallax observations. *The Astrophysical Journal* **561**, 930–937.

Carlson BE, Lehtinen NG and Inan U (2010) Neutron production in terrestrial gamma ray flashes. *Journal of Geophysical Research* **115**, 6.

Cha AN, Sembach KR and Danks AC (1999) The distance to the Vela supernova remnant. *The Astrophysical Journal Letters* **515**, L25–L28.

Chevalier RA (1992) Supernova 1987A at five years of age. *Nature* **355**, 691–696.

Churazov E, Sunyaev R, Isern J, Bikmaev I, Bravo E and Al E (2015) Gamma rays from Type Ia supernova SN 2014. *The Astrophysical Journal* **812**, 1–17.

Clark DH, Mccrea WH and Stephenson J (1977) Frequency of nearby supernovae and climatic and biological catastrophes. *Nature* **265**, 318–319.

Colgate SA (1975) The prompt effects of supernovae. *Annals of the New York Academy of Sciences* **262**, 34–46.

Cristofari P, Renaud M, Marcowith A, Dwarkadas VV and Tatischeff V (2020) Time-dependent high-energy gamma-ray signal from accelerated particles in core-collapse supernovae: the case of SN 1993. *Journal of Monthly Notices of the Royal Astronomical Society* **494**, 2760–2765.

Damon PE, Kaimei D, Kocharov G, Mikheeva I and Peristykh A (1995) Radiocarbon production by the gamma-ray component of supernova explosions. *Radiocarbon* **37**, 599–604.

Dee M, Pope B, Miles D, Manning S and Miyake F (2016) Supernovae and single/year anomalies in the atmospheric radiocarbon record. *Radiocarbon* **59**, 1–10.

Dodson R, Legge D, Reynolds JE and Mcculloch PM (2003) The Vela pulsar's proper motion and parallax derived from VLBI observations. *The Astrophysical Journal* **596**, 1137–1141.

Duggan P, McBreen B, Hanlon L, Metcalfe L, Kvick A and Vaughan G (2001) The effects of a gamma-ray burst on nearby preplanetary systems. *ESO Symposia: Gamma-Ray Bursts in Afterglow*. Heidelberg: Spring-Verlag Berlin, pp. 294–296.

Eastoe CJ, Tucek CS and Touchan R (2019) Δ14C and δ13C in annual tree-ring samples from Sequoiadendron Giganteum, AD 998–1510: solar cycles and climate. *Radiocarbon* **61**, 661–680.

Fahrni SM, Southon J, Fuller BT and Park J (2020) Single-year German Oak and Calfornian Bristlecone Pine 14C data at the beginning of the Hallstatt Plateau from 856 BC to 626 BC. *Radiocarbon* **16**, 919–937.

Faith JT and Surovell TA (2009) Synchronous extinction of North America's Pleistocene mammals. *Proceedings of the National Academy of Sciences* **106**, 20641–20645.

Farrand G and Safi-Harb S (2012) A census of high-energy observations of galactic supernova remnants. *Advances in Space Research* **49**, 1313–1319. Available at http://www.physics.umanitoba.ca/snr/SNRcat/.

Fesen RA, Neustadt JMM, Black C and Milisavljevic D (2018*a*) A distance estimate to the Cygnus Loop based on the distances to two stars located within the remnant. *Monthly Notices of the Royal Astronomical Society* **475**, 3996–4010.

Fesen RA, Weil KE, Cisneros IA, Blair WP and Raymond JC (2018*b*) The Cygnus Loop's distance, properties, and environment driven morphology. *Monthly Notices of the Royal Astronomical Society* **481**, 1786–1798.

Fesen R, Kremer R, Patnaude D and Milisavljevic D (2011) The SN 393–SNR RX J1713.7-3946 (G347.3-0.5) connection. *Astronomical Journal* **143**, 27 (6pp).

Fishman GJ and Inan US (1988) Observation of an ionospheric disturbance caused by a gamma-ray burst. *Nature* **331**, 418–420.

Foster TJ, Cooper B, Reich W, Kothes R and West J (2013) Two radio supernova remnants discovered in the outer Galaxy. *Astronomy and Astrophysics* **549**, 9.

Fox AC, Eigenbrode JL, Pavlov A and Lewis J (2017) *The Effect of Gamma Radiation on Mars Mineral Matrices: Implications for Perchlorate Formation on Mars*. American Geophysical Union, Fall Meeting 2017, San Francisco, USA.

Galante D and Horvath JE (2007) Biological effects of gamma-ray bursts: distances for severe damage on the biota. *International Journal of Astrobiology* **6**, 19–26.

Gao XY, Reich P, Reich W, Hou LG and Han JL (2020) Discovery of a new supernova remnant G21.8-3.0. *Monthly Notices of the Royal Astronomical Society* **493**, 2188–2194.

Gehrels N and Mészáros P (2012) Gamma ray bursts. *Science* **337**, 932.

Gehrels N, Laird CM, Jackman CH, Cannizzo JK and Mattson BJ (2003) Ozone depletion from nearby supernovae. *The Astrophysical Journal*, **585**, 1169–1176.

Gowanlock MG (2016) Astrobiological effects of gamma-ray bursts in the Milky Way Galaxy. *The Astrophysical Journal* **832**, 12.

Green DA (2019) A revised catalogue of 294 Galactic supernova remnants. *Journal of Astrophysics and Astronomy* **40**, 12 pp.

Hamuy M and Pinto PA (2002) Type II supernovae as standardized candles. *The Astrophysical Journal Letters* **566**, L63–L65.

Hayakawa H, Tamazawa H, Uchiyama Y, Ebihara Y, Miyahara H, Kosaka S, Iwahashi K and Isobe H (2017) Historical auroras in the 990s: evidence for great magnetic storms. *Solar Physics* **292**, 12.

Horvath JE and Galante D (2012) Effects of high-energy astrophysical events on habitable planets. *International Journal of Astrobiology* **11**, 279–286.

Hua Q and Al E (2009) Atmospheric 14C variations derived from tree rings during the early Younger Dryas. *Quaternary Science Reviews* **28**, 2982–2990.

Hughen KA, Southon JR, Lehman SJ and Overpeck JT (2000) Synchronous radiocarbon and climate shifts during the last deglaciation. *Science* **290**, 1951–1954.

Inan US, Lehtinen NG, Moore RC, Hurley K, Boggs S, Smith DM and Fishman GJ (2007) Massive disturbance of the daytime lower ionosphere by the giant γ-ray flare from magnetar SGR 1806–20. *Geophysical Research Letters* **34**, L08103 (5 pp).

Jiang S-Y and Zhao F-Y (2007) The historical re-brightening and distance recheck of SN 1006. *Chinese Journal of Astronomy and Astrophysics* **7**, 325–328.

Jull AJT, Panyushkina I, Miyake F, Masuda K, Nakamura T, Mitsutani T, Lange TE, Cruz RJ, Baisan C, Janovics R, Varga T and Molnár M (2018) More rapid 14C excursions in the tree-ring record: a record of different kind of solar activity at about 800 BC?. *Radiocarbon* **60**, 1237–1248.

Jull AJT, Panyushkina IP, Molnár M, Varga T, Wacker L, Brehm N, Baisan C, Salzer MW and Tegel W (2020) Rapid 14C excursion at 3372-3371 BCE

https://doi.org/10.1017/S1473550420000348 Published online by Cambridge University Press

not observed at two different locations – comment on Wang *et al.* (2017). arXiv:2003.09387 [physics.geo-ph].

Kann DA, Schady P, Olivares FE, Klose S, Rossi A, Perley DA, Krühler T, Greiner J, Nicuesa Guelbenzu A, Elliott J, Knust F, Filgas R, Pian E, Mazzali P, Fynbo JPU, Leloudas G, Afonso PMJ, Delvaux C, Graham JF, Rau A, Schmidl S, Schulze S, Tanga M, Updike AC and Varela K (2019) Highly luminous supernovae associated with gamma-ray bursts, 1, GRB 111209A/SN 2011kl in the context of stripped-envelope and superluminous supernovae. *Astronomy and Astrophysics* **624**, A143 (19 pp.).

Kanu AM, Comfort LL, Guilderson TP, Cameron-Smith PJ, Bergmann DJ, Atlas EL, Schauffler S and Boering KA (2016) Measurements and modeling of contemporary radiocarbon in the stratosphere. *Geophysical Research Letters* **43**, 1399–1406.

Kasen D and Woosley SE (2009) Type II supernovae: model light curves and standard candle relationships. *The Astrophysical Journal* **703**, 2205–2216.

Klein RI and Chevalier RA (1978) X-ray bursts from Type II supernovae. *The Astrophysical Journal* **223**, L109–L112.

Kothes R (2003) G107.5-1.5, a new SNR discovered through its highly polarized radio emission. *Astronomy and Astrophysics* **408**, 187–192.

Kovaltsov GA, Mishev A and Usoskin IG (2013) A new model of cosmogenic production of radiocarbon 14C in the atmosphere. *Earth and Planetary Science Letters* **337–338**, 114–120.

Kudsk SGK, Philippsen B, Baittinger C and Fogtmann-Schulz A (2019) New single-year radiocarbon measurements based on Danish oak covering the periods AD 692–790 and 966–1057.

Leahy DA and Tian WW (2007) Radio spectrum and distance of the SNR HB9. *Astronomy & Astrophysics* **461**, 1013–1018.

Lingenfelter RE and Ramaty R (1970) Astrophysical and geophysical variation in C-14 production. In Olsson IU (ed). *Radiocarbon Variations and Absolute Chronology*. New York: John Wiley and Sons, pp. 513–537.

Lopez LA, Ramirez-RUIZ E, Castro D and Pearson S (2013) The galactic supernova remnant W49B likely originates from a jet-driven, core-collapse explosion. *The Astrophysical Journal* **764**, 50 (5pp).

Lovett RA (2012) Ancient text gives clue to mysterious radiation spike. *Nature* **486**. doi:10.1038/nature.2012.10898.

Mangerud J, Briner JP, Goslar T and Svendsen JI (2017) The bølling-age blomvåg beds, western Norway: implications for the Older Dryas glacial re-advance and the age of the deglaciation. *Boreas* **46**, 162–184.

Martín O, Galante D, Cárdenas R and Horvath JE (2009) Short-term effects of gamma ray bursts on Earth. *Astrophysics and Space Science* **321**, 161–167.

Matz SM, Share GH, Leising MD, Chupp EL, Vestrand WT, Purcell WR, Strickman MS and Reppin C (1988) Gamma-ray line emission from SN1987A. *Nature* **331**, 416–418.

Mekhaldi F, Muscheler R, Adolphi F, Aldahan A, Beer J, McConnell JR, Possnert G, Sigl M, Svensson A, Synal H-A, Welten KC and Woodruff TE and Others A (2015) Multiradionuclide evidence for the solar origin of the cosmic-ray events of AD 774/5 and 993/4. *Nature Communications* **6**, 8611 (8 pp).

Melott A, Lieberman B, Laird C, Martin L, Medvedev M, Thomas B, Cannizzo J, Gehrels N and Jackman CH (2003) Did a gamma-ray burst initiate the late Ordovician mass extinction?.

Melott AL, Thomas BC, Hogan DP, Ejzak LM and Jackman CH (2005) Climatic and biogeochemical effects of a galactic gamma ray burst. *Geophysical Research Letters* **32**, L14808 (5 pp).

Menjo H, Miyahara H, Kuwana K, Masuda K, Muraki Y and Nakamura T (2005). Possibility of the detection of past supernova explosion by radiocarbon measurement. Acharya BS (ed.) *Proceedings of the 29th International Cosmic Ray Conference*. Mumbai: Tata Institute of Fundamental Research.

Miyake F, Nagaya K, Masuda K and Nakamura T (2012) A signature of cosmic-ray increase in AD 774–775 from tree rings in Japan. *Nature* **486**, 240–242.

Miyake F, Masuda K and Nakamura T (2013) Another rapid event in the carbon-14 content of tree rings. *Nature Communications* **4**, 1748.

Miyake F, Masuda K, Nakamura T, Kimura K, Hakozaki M, Jull AJT, Lange TE, Cruz R, Panyushkina IP, Baisan C and Salzer MW (2016) Search for annual 14C excursions in the past. *Radiocarbon* **59**, 315–320.

Miyake F, Jull AJT, Panyushkinad IP, Wackere L, Salzerd M and Baisand CH (2017) Large 14C excursion in 5480 BC indicates an abnormal sun in the mid-Holocene. *Proceedings of the National Academy of Sciences* **114**, 881–884.

Moriya TJ, Sorokina EI and Chevalier RA (2018) Superluminous supernovae. *Space Science Reviews* **214**, 59 (37 pp).

Nakar E and Sari R (2010) Early supernovae light curves following the shock breakout. *The Astrophysical Journal* **725**, 904–921.

Nakar E and Sari R (2012) Relativistic shock breakouts-a variety of gamma-ray flares: from low-luminosity gamma-ray bursts to type Ia supernovae. *The Astrophysical Journal* **747**, 15.

Neuhäuser R and Hambaryan VV (2014) A solar super-flare as cause for the 14C variation in AD 774/5?. *Astronomische Nachrichten* **335**, 949–963.

Olivier M, Stocker TF and Muscheler R (2001) Atmospheric radiocarbon during the Younger Dryas: production, ventilation, or both?. *Earth and Planetary Science Letters* **281**, 383–395.

Pavlov AK, Vdovina MA, Vasilyev GI, Pavlov AK, Blinov AV, Ostryakov VM, Konstantinov AN and Volkov PA (2013) AD 775 Pulse of cosmogenic radionuclides production as imprint of a galactic gamma-ray burst. *Monthly Notices of the Royal Astronomical Society* **435**, 2878–2884.

Pavlovic MC, Dobardzic A, Vukotic B and Urosevic D (2014) Updated radio Σ–D relation for galactic supernova remnants. *Serbian Astronomical Journal* **189**, 1–5.

Pearson C, Wacker L, Bayliss A, Brown D, Salzer M, Brewer P, Bollhalder S, Boswijk G and Hodgins G (2020) Annual variation IN atmospheric 14C between 1700 BC and 1480 BC. *Radiocarbon* **62**, 939–952.

Pian E, Mazzali PA and Starling R (2006) An optical supernova associated with the X-ray flash XRF 060218. *Nature* **442**, 1011–1017.

Pinto PA and Woosley SE (1988) The theory of gamma-ray emergence in supernova 1987A. *Nature* **333**, 534–537.

Piran T and Jimenez R (2014) Possible role of gamma ray bursts on life extinction in the universe. *Physical Review Letters*, **113**, 231102 (6 pp).

Podsiadlowski P (2013) Supernovae and gamma ray bursts. In Oswalt TD and Barstow MA (eds). *Planets, Stars, and Stellar Systems*. Dordrecht: Springer, pp. 693–733.

Reimer P (2013) Intcal13 and Marine13 radiocarbon age calibration curves 0–50,000 years cal BP. *Radiocarbon* **55**, 1869–1887.

Renssen H, Van Geel B, Van Der Plicht J and Magny M (2000) Reduced solar activity as a trigger for the start of the Younger Dryas?. *Quaternary International* **68**, 373–383.

Rood RT, Sarazin CL, Zeller EJ and Parker BC (1979) X or Y rays from supernovae in glacial ice. *Nature* **282**, 701–702.

Ruderman MA (1974) Possible consequences of nearby supernova explosions for atmospheric ozone and terrestrial life. *Science* **184**, 1079–1081.

Safi-Harb S, Ferrand G and Matheson H (2012) *A high-energy catalogue of galactic supernova remnants and pulsar wind nebulae*. In Leeuwen JV (ed.), *Neutron Stars and Pulsars: Challenges and Opportunities after 80 years. Proceedings, IAU Symposium No. 291*.

Sakurai H, Tokanai F, Miyake F, Horiuchi K, Masuda K, Miyahara H, Ohyama M, Sakamoto M, Mitsutani T and Moriya TJ (2020) Prolonged production of 14C during the ~660 BCE solar proton event from Japanese tree rings. *Scientific Reports* **10,** (7 pp).

Scalo J and Wheeler JC (2002) Astrophysical and astrobiological implications of gamma-ray burst properties. *The Astrophysical Journal* **566**, 723–737.

Scifo A, Kuitems M, Neocleous A, Pope BJS, Miles D, Jansma E, Doeve P, Smith AM, Miyake F and Dee MW (2019) Radiocarbon production events and their potential relationship with the Schwabe cycle. *Scientific Reports* **9**, 17056 (8 pp).

Siegenthaler U, Heimann M and Oeschger H (1980) 14C Variations caused by changes in the global carbon cycle. *Radiocarbon* **22**, 177–191.

Sigl M, Winstrup M and Al E (2015) Timing and climate forcing of volcanic eruptions for the past 2,500 years. *Nature* **523**, 543–549.

Southon J, Noronha AL, Cheng H, Edwards RL and Wang Y (2012) A high-resolution record of atmospheric 14C based on Hulu Cave speleothem H82. *Quaternary Science Reviews* **33**, 32–41.

Stephenson FR (2015) Astronomical evidence relating to the observed 14C increases in A.D. 774–5 and 993–4 as determined from tree rings. *Advances in Space Research* **55**.

https://doi.org/10.1017/S1473550420000348 Published online by Cambridge University Press

Stuiver M (1961) Variations in radiocarbon concentration and sunspot activity. *Journal of Geophysical Research* **66**, 273–276.

Stuiver M and Polach HA (1977) Discussion: reporting of 14C data. *Radiocarbon* **19**, 355–363.

Sukhodolov T, Usoskin I, Rozanov E, Asvestari E, Ball WT, Curran MAJ, Fischer H, Kovaltsov G, Miyake F, Peter T, Plummer C, Schmutz W, Severi M and Traversi R (2017) Atmospheric impacts of the strongest known solar particle storm of 775 AD. *Scientific Reports* **7**, 45257 (9 pp).

Sushch I and Hnatyk B (2014) Modelling of the radio emission from the Vela supernova remnant. *Astronomy and Astrophysics* **561**, 8.

Tanaka YT, Terasawa M, Yoshida T and Hayakawa HM (2008) Ionospheric disturbances caused by SGR 1900+14 giant gamma ray flare in 1998: constraints on the energy spectrum of the flare. *Journal of Geophysical Research: Space Physics* **113**, A07307 (7 pp).

Terry KD and Tucker WH (1968) Biologic effects of supernovae. *Science* **159**, 421.

Thomas BC (2009) Gamma-ray bursts as a threat to life on Earth. *International Journal of Astrobiology* **8**, 183–186.

Thomas BC, Melott AL, Jackman CH, Laird CM, Medvedev MV, Stolarski RS, Gehrels N, Cannizzo JK, Hogan DP and Ejzak LM (2005) Gamma-ray bursts and the Earth: exploration of atmospheric, biological, climatic, and biogeochemical effects. *The Astrophysical Journal* **634**, 509–533.

Thorsett S (1995) Terrestrial implications of cosmological gamma-ray burst models. *Astrophysical Journal Letters* **444**, L53 (6pp).

Tsuji N and Uchiyama Y (2016) Expansion measurements of supernova remnant RX J1713.7-3946. *Publications of the Astronomical Society of Japan* **68**, 1–12.

Usoskin IG, Kromer B, Ludlow F, Beer J, Friedrich M, Kovaltsov GA, Solanki SK and Wacker L (2013) The AD775 cosmic event revisited: the Sun is to blame. *Astronomy Astrophysical Letters* **552**, L3 (4 pp).

Wallerstein G and Silk J (1971) Interstellar gas in the direction of the Vela pulsar. *The Astrophysical Journal* **170**, 28.

Wang FY, Yu H, Zou YC, Dai ZG and Cheng KS (2017) A rapid cosmic-ray increase in BC 3372–3371 from ancient buried tree rings in China. *Nature Communications* **8**, 1487.

Wang K, Huang TQ and Zhuo L (2019*a*) Transient high-energy gamma-rays and neutrinos from nearby type II supernovae. *The Astrophysical Journal* **872**, 157–163.

Wang X, Fields BD and Lien AY (2019*b*) Using gamma ray monitoring to avoid missing the next Milky Way type Ia supernova. *Monthly Notices of the Royal Astronomical Society* **486**, 2910–2918.

Wang FY, Yu H, Zou YC, Dai ZG and Cheng KS (2020) Reply to 'Rapid 14C excursion at 3372-3371 BCE not observed at two different locations'. Preprint, arXiv.org > astro-ph > arXiv:2003.11295.

Yar-Uyaniker A, Uyaniker B and Kothes R (2004) Distance of three supernova remnants from H I line observations in a complex region: G114.3+0.3, G116.5 +1.1, and CTB 1 (G116.9+0.2). *The Astrophysical Journal* **616**, 247–256.

Yuan Q, Liao N-H, Xin Y-L, Li Y, Fan Y-Z, Zhang B, Hu H-B and Bi X-J (2018) Fermi Large Area Telescope detection of gamma-ray emission from the direction of Supernova iPTF14hls. *The Astrophysical Journal Letters* **854**, L18 (5 pp).

Zhu H and Tian W (2013) Distances of Galactic supernova remnants. In Ray A. and Mcscray RAE (ed), *Supernova Environmental Impacts*. Proceedings of the International Astronomical Union **9**(S296), 378–379.

https://doi.org/10.1017/S1473550420000348 Published online by Cambridge University Press